

Structural Modification on Tetraphenylpyrazine: from Polarity Enhanced Emission to Polarity Quenching Emission and Its Intramolecular Charge Transfer Mechanism

Haozhong Wu, Lili Du, Juanjuan Luo, Zhiming Wang,* David Lee Phillips,* Anjun Qin and Ben Zhong Tang

Part 1. General Information

¹H and ¹³C NMR spectra were measured on a VNMRS spectrometer. High resolution mass spectra (HRMS) were recorded on an Agilent1290/Bruker maXis impact mass spectrometer. Absorption spectrum were tested on a Shimadzu UV-2600 spectrophotometer. Photoluminescence (PL) spectra were measured on a Horiba Fluoromax-4 spectrofluorometer. Fluorescence quantum yields were characterized using a Hamamatsu absolute PL quantum yield spectrometer C11347 Quantaaurus QY. Fluorescence lifetimes were determined with a Hamamatsu C11367-11 Quantaaurus-Tau time-resolved spectrometer.

Part 2. Computational Methodology

The geometry optimization and energy calculation were performed at M06-2X/6-31g (d,p) level with polarizable continuum model (PCM) in the Gaussian 16 package. The Linear-response PCM was used in geometry optimization and frontier molecular orbitals analysis, while the state-specific PCM was employed to the energy calculation. Then the natural transition orbitals (NTOs), hole-electron research and transition density matrix were analyzed in Multiwfn program.

The equations and definitions detail of hole-electron distribution.

These parameters are obtained by the following equation defined by Multiwfn program. To investigate which MOs (Molecule orbital) have significant contributions to hole and electron, the contribution of occupied MO to hole and contribution of virtual MO to electron were defined as follows. The data can reflect which molecular orbitals play an important role in the transition. Therefore, it is convenient for quantitative analysis and discussion.

$$\Theta_i^{hole} = \sum_a [(w_i^a)^2 - (w_i'^a)^2] \quad \Theta_i^{ele} = \sum_a [(w_i^a)^2 - (w_i'^a)^2]$$

where i , a , w and w' respectively represent occupied MOs, virtual MOs, configuration coefficient of excitation and configuration coefficient of de-excitation.

below normalization conditions are held evidently

$$\sum_i \Theta_i^{hole} = 1 \quad \sum_a \Theta_a^{ele} = 1$$

Contribution to hole/electron by an atom can be derived as follows. Considering the normalization condition of the hole (de-excitation part is temporarily ignored for simplicity).

$$\int \left(\sum_{i,j \rightarrow a} w_i^a w_j^a \varphi_i \varphi_j \right) dr = 1$$

$$\int \left(\sum_{i,j \rightarrow a} w_i^a w_j^a \sum_{\mu} \sum_{\nu} C_{\mu,i} C_{\nu,j} \chi_{\mu} \chi_{\nu} \right) dr = 1$$

$$\sum_{i,j \rightarrow a} w_i^a w_j^a \sum_{\mu} \sum_{\nu} C_{\mu,i} C_{\nu,j} \int \chi_{\mu} \chi_{\nu} dr = 1$$

$$\sum_{i,j \rightarrow a} w_i^a w_j^a \sum_{\mu} \sum_{\nu} C_{\mu,i} C_{\nu,j} S_{\mu,\nu} = 1$$

where χ denotes basis function, S and C are overlap matrix and coefficient matrix, and μ and ν represent basis function respectively. Mulliken-like method are employed to

partition the term $\sum_{\mu} \sum_{\nu} C_{\mu,i} C_{\nu,j} S_{\mu,\nu}$ as atomic contributions, then the contribution of atom A to hole are defined in below form.

$$\Theta_A^{hole} = \sum_{i,j \rightarrow a} w_i^a w_j^a \frac{1}{2} \left(\sum_{\mu \in A} \sum_{\nu} C_{\mu,i} C_{\nu,j} S_{\mu,\nu} + \sum_{\mu} \sum_{\nu \in A} C_{\mu,i} C_{\nu,j} S_{\mu,\nu} \right)$$

Apply above treatment on de-excitation part of hole as well as electron. The actual equations used to evaluate atomic contribution to hole and electron are

$$\Theta_A^{hole} = \sum_{i,j \rightarrow a} w_i^a w_j^a \frac{1}{2} \left(\sum_{\mu \in A} \sum_{\nu} T_{\mu,\nu}^{ij} + \sum_{\mu} \sum_{\nu \in A} T_{\mu,\nu}^{ij} \right) - \sum_{i,j \rightarrow a} w_i^a w_j^a \frac{1}{2} \left(\sum_{\mu \in A} \sum_{\nu} T_{\mu,\nu}^{ij} \right)$$

$$\Theta_A^{ele} = \sum_{i \rightarrow a,b} w_i^a w_i^b \frac{1}{2} \left(\sum_{\mu \in A} \sum_{\nu} T_{\mu,\nu}^{ab} + \sum_{\mu} \sum_{\nu \in A} T_{\mu,\nu}^{ab} \right) - \sum_{i \rightarrow a,b} w_i^a w_i^b \frac{1}{2} \left(\sum_{\mu \in A} \sum_{\nu} T_{\mu,\nu}^{ab} \right)$$

$$T_{\mu,\nu}^{ij} = C_{\mu,i} C_{\nu,j} S_{\mu,\nu}$$

Fragment contribution to hole and electron can be simply evaluated by summing up atomic contributions

$$\Theta_{frag}^{hole} = \sum_{A \in frag} \Theta_A^{hole} \quad \Theta_{frag}^{ele} = \sum_{A \in frag} \Theta_A^{ele}$$

Overlap between hole and electron in atom and fragment spaces are defined as geometry average of their contributions:

$$\Theta_A^{ovlp} = \sqrt{\Theta_A^{ele} \Theta_A^{hole}} \quad \Theta_{frag}^{ovlp} = \sqrt{\Theta_{frag}^{ele} \Theta_{frag}^{hole}}$$

Therefore, the percentages of hole-electron overlap on TPP are obtained by follow equation.

$$\Theta_{TPP}^{ovlp} = \sqrt{\Theta_{TPP}^{ele} \Theta_{TPP}^{hole}}$$

3) The equations and definitions detail of TDM.

$$P_{\mu\nu}^{tran} = \sum_i^{occ} \sum_a^{vir} w_i^a C_{\mu i} C_{\nu a}$$

$$T(r;r') = \sum_{\mu} \sum_{\nu} P_{\mu\nu}^{tran} \chi_{\mu}(r) \chi_{\nu}(r')$$

$C_{\mu i}$ denotes the expansion coefficient of basis function μ in MO i . χ denotes basis function.

The off-diagonal elements of TDM essentially represent the coupling between various basis functions during electron excitation. Assume there are only two basic functions and meantime the excitation can be perfectly represented as $i \rightarrow a$ MO transition, then the TDM could be explicitly written as below form.

$$P^{tran} = \begin{bmatrix} 1,2 & 2,2 \\ 1,1 & 2,1 \end{bmatrix} = \begin{bmatrix} C_{1i}C_{2a} & C_{2i}C_{2a} \\ C_{1i}C_{1a} & C_{2i}C_{1a} \end{bmatrix}$$

The TDM can be contracted to atoms based on form according to correspondence between basis functions and atoms, it will be symbolized as \mathbf{p} .

$$p_{AB} = \sum_{\mu \in A} \sum_{\nu \in B} (P_{\mu\nu}^{tran})^2$$

μ and ν represent the basic functions centered at atom A and on B. the general structure of the resulting \mathbf{p} could be expressed in below form

$$p = \begin{bmatrix} 1,N & \cdots & N,N \\ \vdots & \ddots & \vdots \\ 1,1 & \cdots & N,1 \end{bmatrix}$$

Diagonal terms: If (A, A) is large, it implies that atom A has large contribution to both hole and electron. Therefore, the electron excitation should result in evident charge reorganization within atom A.

Off-diagonal terms: If (A, B) is large, then atom A should have large contribution to hole and meantime atom B should have large contribution to electron, implying that electron excitation leads to CT from A to B.

If fragments are defined, the p (or other kinds of atom transition matrix) can further be contracted to fragment based on form:

$$p_{RS} = \sum_{A \in \text{frag } R} \sum_{B \in \text{frag } S} p_{AB}$$

Therefore, the transition density matrix (TDM) of $\{X, Y\}$ are computed by the equation.

$$p_{XY} = \sum_{A \in \text{frag } X} \sum_{B \in \text{frag } Y} p_{AB}$$

Part 3. Synthesis procedure

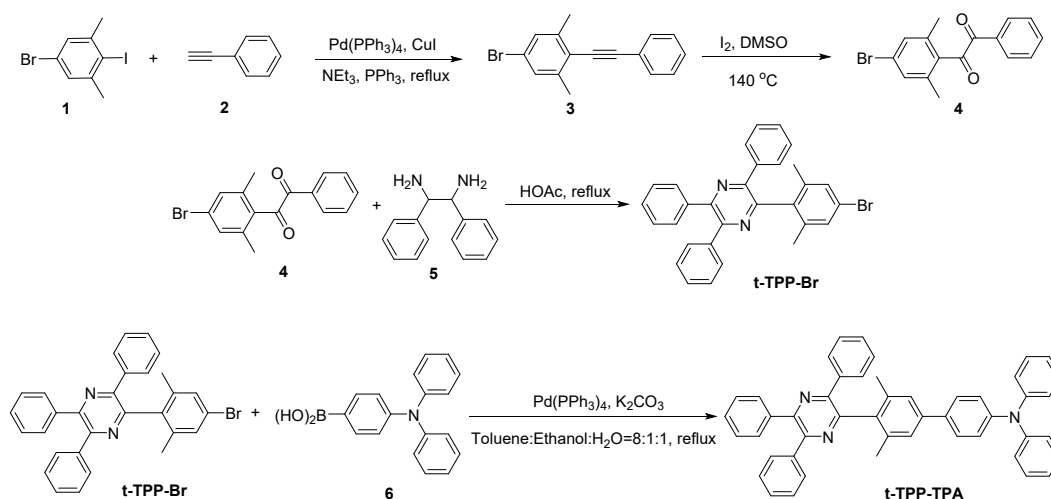


Figure S1. Synthetic route of five target compounds.

5-bromo-1,3-dimethyl-2-(phenylethynyl)benzene (3): A mixture of 5-bromo-2-iodo-1,3-dimethylbenzene (**1**) (8.0 mmol, 2.48 g), CuI (0.16 mmol, 0.04 g), $\text{Pd}(\text{PPh}_3)_4$ (0.08 mmol, 0.11 g) and triphenylphosphine (0.64 mmol, 0.17 g) was added in 100 mL two-neck bottle under nitrogen. After then, the liquid reactant phenylacetylene (**2**) (10 mmol, 1.10 mL), triethylamine and THF was injected into the bottle and the mixture was refluxed overnight under nitrogen atmosphere. After cooling to room temperature, the solvent was removed under reduced pressure and solid was dissolved into dichloromethane and washed with brine and water, successively. And then, the organic solution was dried over MgSO_4 . The solvent was removed under reduced pressure and

the crude product was purified by column chromatography, yield is 45%. ¹H NMR (400 MHz, CD₂Cl₂) δ (TMS, ppm): 7.56–7.51 (m, 2H), 7.40–7.34 (m, 3H), 7.24 (s, 2H), 2.48 (s, 6H). ¹³C NMR (101 MHz, CD₂Cl₂) δ (TMS, ppm): 142.6, 131.7, 130.0, 128.8, 123.8, 122.5, 122.0, 99.1, 86.4, 21.0.

1-(4-bromo-2,6-dimethylphenyl)-2-phenylethane-1,2-dione (4): A mixture of **3** (3.0 mmol, 0.85 g), I₂ (0.06 mmol, 0.15 g) and 10 mL DMSO. The mixture was rapidly stirred at 140 °C for 4 h. The Na₂S₂O₃ saturated aqueous solution were added into the mixture until the solution became clear. The organic layer was separated and washed with brine and water, and dried over MgSO₄. Evaporation of the solvent afforded nearly pure compound, yield is 58%. ¹H NMR (400 MHz, CD₂Cl₂) δ (TMS, ppm): 8.16–8.10 (m, 2H), 7.74–7.68 (m, 1H), 7.60–7.54 (m, 2H), 7.28 (d, *J* = 0.5 Hz, 2H), 2.25 (s, 6H). ¹³C NMR (101 MHz, CD₂Cl₂) δ (TMS, ppm): 197.4, 191.2, 139.3, 136.0, 135.2, 132.3, 131.6, 130.8, 129.4, 125.3, 20.5. HRMS (MALDI-TOF): *m/z* [M⁺] calcd. for C₁₆H₁₃O₂Br, 316.0099. found, 316.0093.

2-(4-bromo-2,6-dimethylphenyl)-3,5,6-triphenylpyrazine (t-TPP-Br): A mixture of **4** (1.5 mmol, 0.47 g), 1,2-diphenylethane 1,2-diamine (1.8 mmol, 0.38 g) and glacial acetic acid (15 mL) were added in 100 mL two-neck bottle and then refluxed under air for 3 h. After cooling down, the solid product was filtrated and washed with methanol. The crude product was purified by column chromatography, yield is 66%. ¹H NMR (400 MHz, CD₂Cl₂) δ (TMS, ppm): 7.65–7.60 (m, 2H), 7.56–7.52 (m, 4H), 7.40–7.25 (m, 11H), 2.02 (s, 6H). ¹³C NMR (101 MHz, CD₂Cl₂) δ (TMS, ppm): 150.6, 150.2, 150.0, 148.8, 139.1, 138.8, 138.0, 137.7, 131.0, 130.3, 130.2, 129.3, 129.1, 129.0, 128.6, 128.5, 122.3, 20.3. HRMS (MALDI-TOF): *m/z* [M⁺] calcd. for C₃₀H₂₃N₂Br; 490.1045. found, 490.1038.

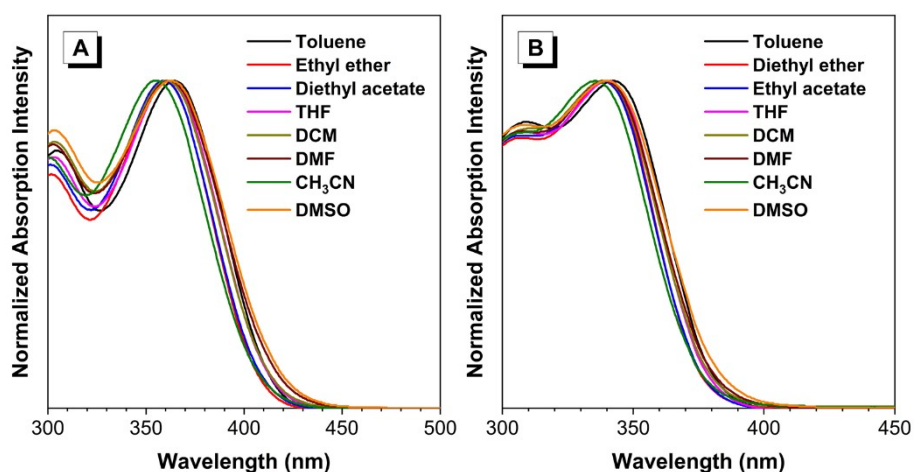
2-(4-bromo-2,6-dimethylphenyl)-3,5,6-triphenylpyrazine (t-TPP-TPA): A mixture of intermediate *t-TPP-Br* (1 mmol, 0.48 g), 4-(diphenylamino)phenylboronic acid (1.5 mmol, 0.43 g), Pd(PPh₃)₄ (0.07 mmol, 0.08 g) and K₂CO₃ (3 mmol, 0.41 g) was added in 100 mL two-neck bottle under nitrogen. After then, a mixed solvent system of toluene/ethanol/water (v/v/v = 8:1:1) 30 mL was injected into the bottle and the mixture was refluxed overnight under nitrogen atmosphere. After cooling to room temperature, the mixture was poured into water and extracted with dichloromethane three times and

the combined organic layers were washed with brine, and then dried over MgSO₄. The solvent was removed under reduced pressure and the crude product was purified by column chromatography, yield was 61%. ¹H NMR (500 MHz, CD₂Cl₂) δ (TMS, ppm): 7.66–7.51 (m, 8H), 7.39–7.24 (m, 15H), 7.11 (dd, *J* = 8.1, 2.9 Hz, 6H), 7.03 (t, *J* = 7.3 Hz, 2H), 2.08 (s, 6H). ¹³C NMR (126 MHz, CD₂Cl₂) δ (TMS, ppm): 150.2, 145.0, 149.9, 149.7, 148.0, 147.4, 140.6, 139.2, 138.8, 138.2, 137.1, 134.7, 130.2, 129.6, 129.1, 128.9, 128.8, 128.5, 128.4, 127.9, 126.3, 124.7, 124.2, 123.3, 20.6. HRMS (MALDI-TOF): *m/z* [M⁺] calcd. for C₄₈H₃₇N₃; 655.2987. found, 655.2981.

Part 4. Femtosecond transient absorption spectra measurement

the fs-TA measurements were accomplished using a femtosecond regenerative amplified Ti: sapphire laser system in which the amplifier was seeded with the 120 fs laser pulses from an oscillator laser system. The laser probe pulse was produced by utilizing ~ 5% of the amplified 800 nm laser pulses to generate a white-light continuum (325–650 nm) in a CaF₂ crystal, and then this probe beam was split into two parts before traversing the sample. The flowing sample was excited by a 267 nm pump laser beam. An absorbance of 1 at 267 nm was used for the sample solutions for the fs-TA experiments in order to maintain the same number of photons being absorbed for the same irradiating conditions for the samples.

Part 5. Supporting data



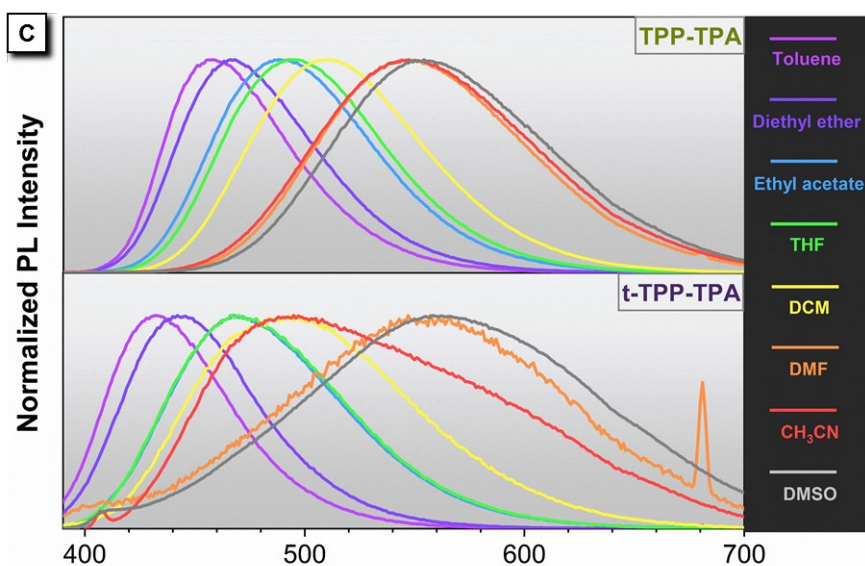


Figure S2. The normalized absorption spectra of TPP-TPA (A) and t-TPP-TPA (B) in different polar solvents (concentration: 10^{-5} M); (C) The normalized PL spectra of TPP-TPA and t-TPP-TPA in different polar solvents (concentration: 10^{-5} M)

Table S1 The photophysical properties of TPP-TPA in different solvents

Solvents	ϵ	n	$f(\epsilon, n)$	λ_a (nm)	λ_f (nm)	$\nu_a - \nu_f$ (cm^{-1})	Φ
Toluene	2.38	1.494	0.014	365	458	5563	0.236
Ethyl ether	4.34	1.352	0.167	359	466	6396	0.229
Ethyl acetate	6.02	1.372	0.2	359	487	7321	0.550
THF	7.58	1.407	0.21	361	495	7499	0.680
DCM	8.93	1.424	0.217	361	509	8054	0.930
DMF	37.0	1.427	0.276	363	547	9267	0.953
CH ₃ CN	37.5	1.344	0.305	355	547	9887	0.815
DMSO	46.7	1.480	0.263	362	553	9541	0.902

Table S2 The photophysical properties of t-TPP-TPA in different solvents

Solvents	ϵ	n	$f(\epsilon, n)$	λ_a (nm)	λ_f (nm)	$\nu_a - \nu_f$ (cm^{-1})	Φ
Toluene	2.38	1.494	0.014	342	433	6145	0.082
Ethyl ether	4.34	1.352	0.167	339	443	6925	0.118
Ethyl acetate	6.02	1.372	0.2	339	470	8222	0.129
THF	7.58	1.407	0.21	340	469	8090	0.165
DCM	8.93	1.424	0.217	338	493	9302	0.115
DMF	37.0	1.427	0.276	339	555	11481	0.053
CH ₃ CN	37.5	1.344	0.305	336	495/580	9560/	0.054
DMSO	46.7	1.480	0.263	339	560	11641	0.061

Table S3. The contrast of the experimental and calculated fluorescence wavelength of TPP-TPA and t-TPP-TPA

	TPP-TPA		t-TPP-TPA	
	exp.	calc.	exp.	calc.
Toluene	458 nm	447 nm	433 nm	425 nm
THF	495 nm	514 nm	469 nm	503 nm
CH ₃ CN	547 nm	572 nm	580 nm	587 nm

Table S4. Selected angles (unit:°) of S₀ and S₁ geometries in three solvents.

	Solvent	State	α_{Py}	α_{Py-A}	α_{Py-B}	α_{Py-C}	α_{Py-D}	α_{D-E}	α_{E-F}
TPP-TPA	Toluene	S ₀	19	39	36	36	39	35	39
		S ₁	35	25	35	29	15	20	30
		Δ	16	-14	-1	-7	-24	-15	-9
	THF	S ₀	19	40	37	37	40	35	38
		S ₁	35	25	37	30	14	18	28
		Δ	16	-15	0	-7	-26	-17	-10
	CH ₃ CN	S ₀	18	41	38	38	40	34	38
		S ₁	35	25	37	30	14	17	27
		Δ	17	-16	-1	-8	-26	-17	-11
t-TPP-TPA	Toluene	S ₀	15	38	40	32	62	36	38
		S ₁	39	24	38	26	39	15	31
		Δ	24	-14	-2	-6	-23	-21	-7
	THF	S ₀	14	39	41	33	63	36	37
		S ₁	27	26	39	27	39	4	30
		Δ	13	-13	-2	-6	-24	-32	-7
	CH ₃ CN	S ₀	14	40	42	34	65	37	35
		S ₁	28	26	40	28	38	12	29
		Δ	14	-14	-2	-6	-27	-25	-6

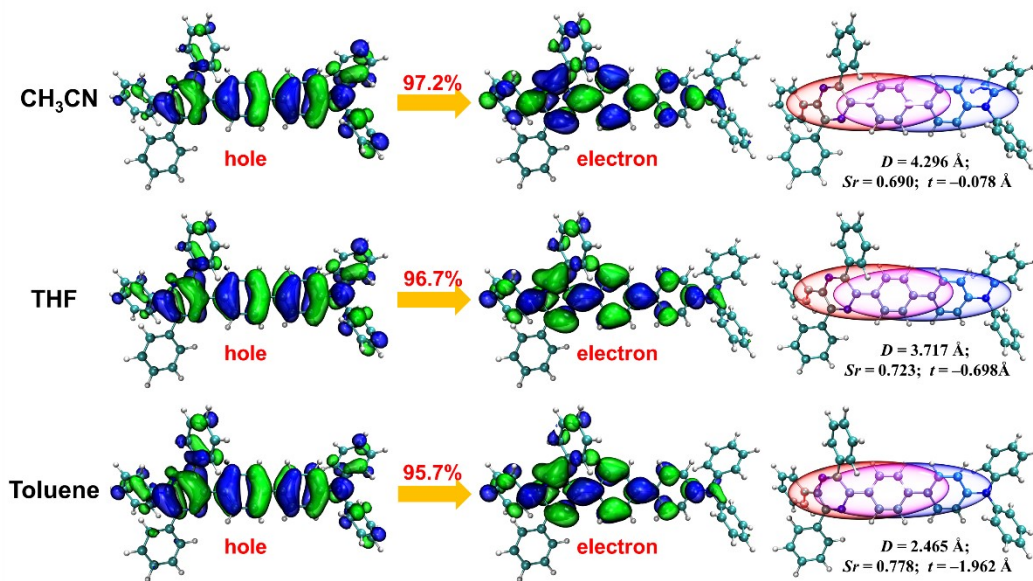


Figure S3. The NTOs and the hole-electron distribution with some parameters of TPP-TPA in three solvents.

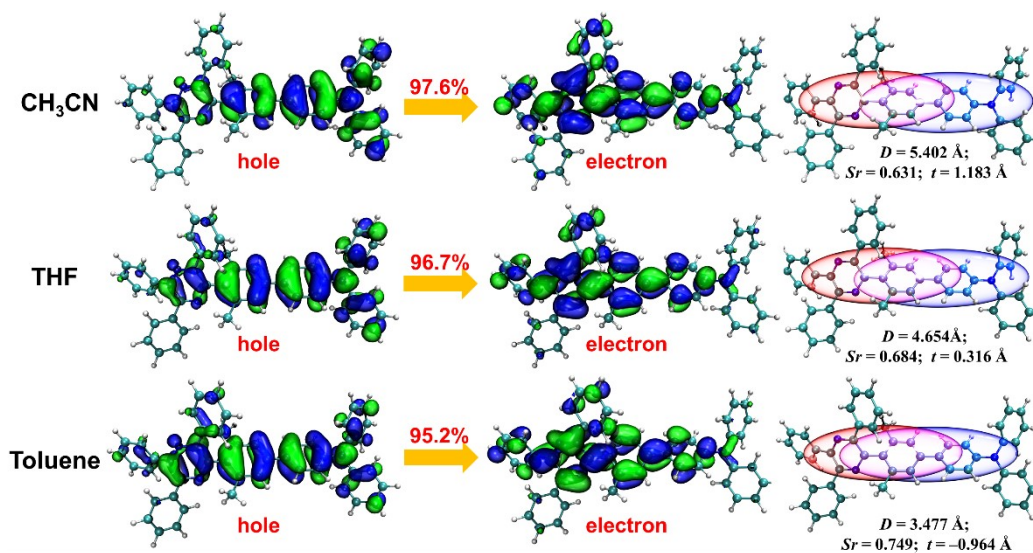


Figure S4. The NTOs and the hole-electron distribution with some parameters of t-TPP-TPA in three solvents

Part 6. Other TPP derivatives

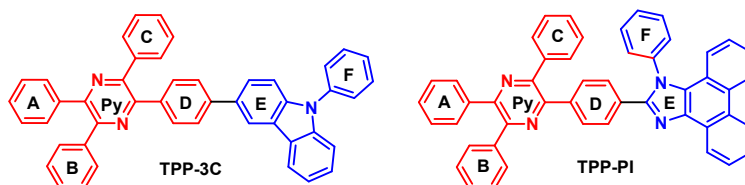


Figure S5. The previously reported TPP compounds with PLICT process and PEE behavior.

According the reported literatures, these TPP structures shown in Figure S5 exhibit

polarity enhanced emission (PEE) solvatochromic phenomenon. Herein, the in-depth calculations are also performed for them, similarly to TPP-TPA and t-TPP-TPA. The calculated S_1 energy levels also match well with the experimental emission peaks for both TPP-3C and TPP-PI (Table S5)

Table S5. The contrast of the experimental and calculated fluorescence wavelength of TPP-3C and TPP-PI

	TPP-3C		TPP-PI	
	exp.	calc.	exp.	calc.
Toluene	441 nm	434 nm	459 nm	441 nm
THF	451 nm	445 nm	464 nm	456 nm
CH ₃ CN	480 nm	454 nm	484 nm	468 nm

Table S6. Selected angles (unit:°) of S_0 and S_1 geometries in three solvents.

	Solvent	State	α_{Py}	α_{Py-A}	α_{Py-B}	α_{Py-C}	α_{Py-D}	α_{D-E}	α_{E-F}
TPP-3C	Toluene	S_0	19	36	36	36	35	37	53
		S_1	42	17	32	24	10	25	53
		Δ	23	-19	-4	-12	-25	-12	0
	THF	S_0	18	37	37	37	36	37	53
		S_1	43	17	33	26	9	23	53
		Δ	25	-20	-4	-11	-27	-14	0
	CH ₃ CN	S_0	18	38	38	38	37	36	53
		S_1	43	16	34	26	9	22	53
		Δ	25	-22	-4	-12	-28	-14	0
TPP-PI	Toluene	S_0	19	36	36	36	35	30	72
		S_1	37	21	34	26	11	10	78
		Δ	18	-15	-2	-10	-24	-20	6
	THF	S_0	19	37	37	37	37	32	72
		S_1	38	21	35	27	10	10	78
		Δ	19	-16	-2	-10	-27	-22	6
	CH ₃ CN	S_0	18	38	38	38	37	32	72
		S_1	38	21	35	27	10	11	78
		Δ	20	-17	-3	-11	-27	-21	6

As shown in Table S6, the S_1 conformations of TPP-3C and TPP-PI also occur to the planarization process similar to TPP-TPA.

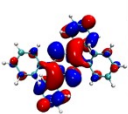
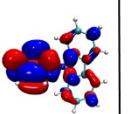
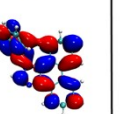
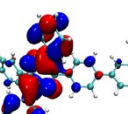
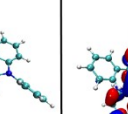
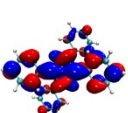
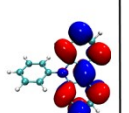
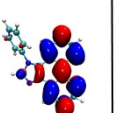
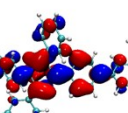
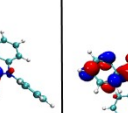
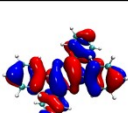
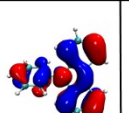
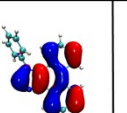
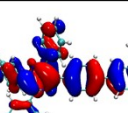
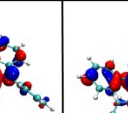
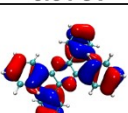
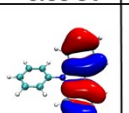
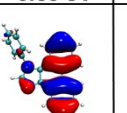
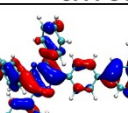
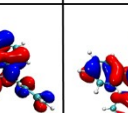
	TPP	3C	PI	TPP-3C	TPP-PI
LUMO + 1	 -0.57 eV	 0.50 eV	 -0.17 eV	 -0.53 eV	 -0.60 eV
LUMO	 -1.50 eV	 -0.17 eV	 -0.32 eV	 -1.50 eV	 -1.62 eV
HOMO	 -6.31 eV	 -6.58 eV	 -6.59 eV	 -6.11 eV	 -6.11 eV
HOMO - 1	 -7.95 eV	 -7.10 eV	 -7.14 eV	 -6.80 eV	 -6.89 eV

Figure S6. The frontier molecular orbitals of D/A units and two target compounds in toluene.

Then, The frontier molecular orbitals of D/A units and target compounds in toluene solvents are analysed (Figure S6). The HOMOs energy of D/A units are close in the range of -6.59 to -6.31 eV, while the LUMOs of donors 3C and PI are much higher than the LUMO of TPP. Combining two parts into the D-A structures, the HOMOs of these TPP derivatives are delocalized on the whole structures because of the proximal HOMOs of two parts. As the too low LUMO of TPP, their LUMOs populate only on the TPP and the adjacent phenyl groups. From these molecular orbitals, these TPP compounds exhibits the larger HOMO-LUMO overlap on TPP units.

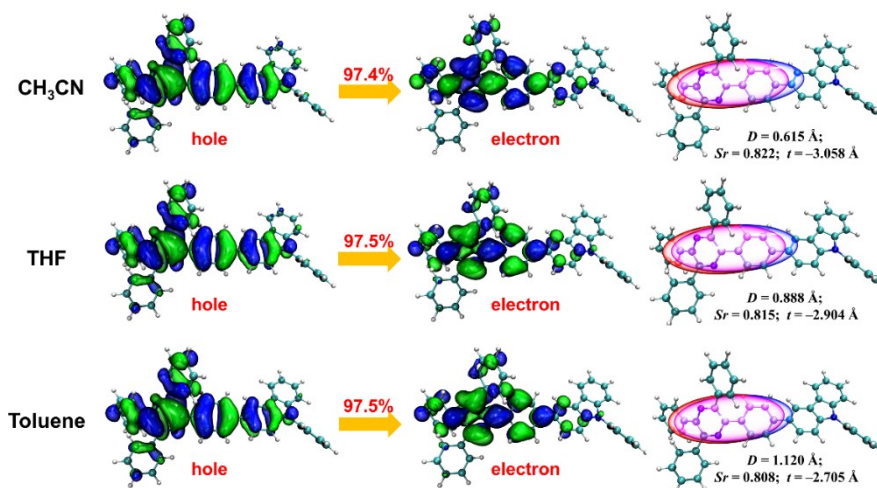


Figure S7. The NTOs and the hole-electron distribution with some parameters of TPP-3C in three solvents.

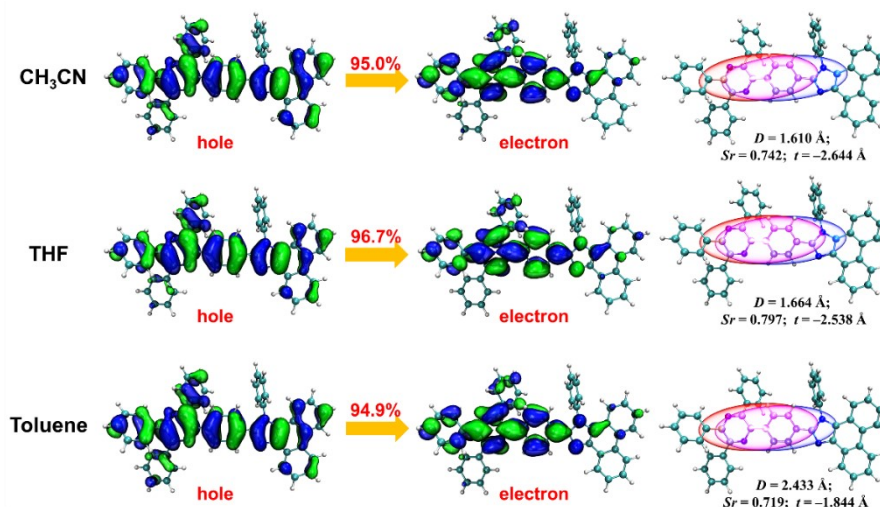


Figure S8. The NTOs and the hole-electron distribution with some parameters of TPP-PI in three solvents.

Next, their natural transition orbitals (NTOs) are analysed to explore the S_1 natures. As illustrated in Figure S7, the holes and electrons of TPP-3C show obvious overlap on TPP and adjacent phenyl groups in three solvents. Similarly, TPP-PI also show remarkable hole-electron overlap, except on the phenyl groups B, F and phenanthrene (Figure S8). As the polarity increases, the larger hole-electron centroid distance (D) and more positive separated parameter (t) suggest their hole-electron distributions are also influenced by the solvents. Interestingly, the overlap parameter (Sr) of TPP-3C becomes small persistently, while that of TPP-PI increases first and then decreases. Therefore, their hole-electron distribution ratios and fragment transition density matrices (TDM) were investigated in three solvents. With the increase of solvent polarity, for TPP-3C (Figure S9A), the hole distribution on Py unit decreases from 36.2% to 32.5% and that on A-D units also decrease in respective extent, but the hole distributes more on donor, especially on carbazole (E unit) increasing from 14.3% to 19.8%; contrarily, the electron distribution changes slightly as the polarity increases, so the hole-electron overlap on TPP reduces while the overlap on carbazole rises in high polarity. The negligible distributions on F unit can be attributed to the large twisting angle and limited conjugation. For TPP-PI, its variations of hole and electron distributions dependent on polarity are different from that of TPP-3C to some extent. It seems that the hole and electron distribution increase on D and E units in THF, but then electron distributes less on D and E units in CH₃CN. These indicate the much delocalized distribution happens priorly in the medium polarity and then partly separated distribution happens in high polarity for TPP-PI (Figure S9B).

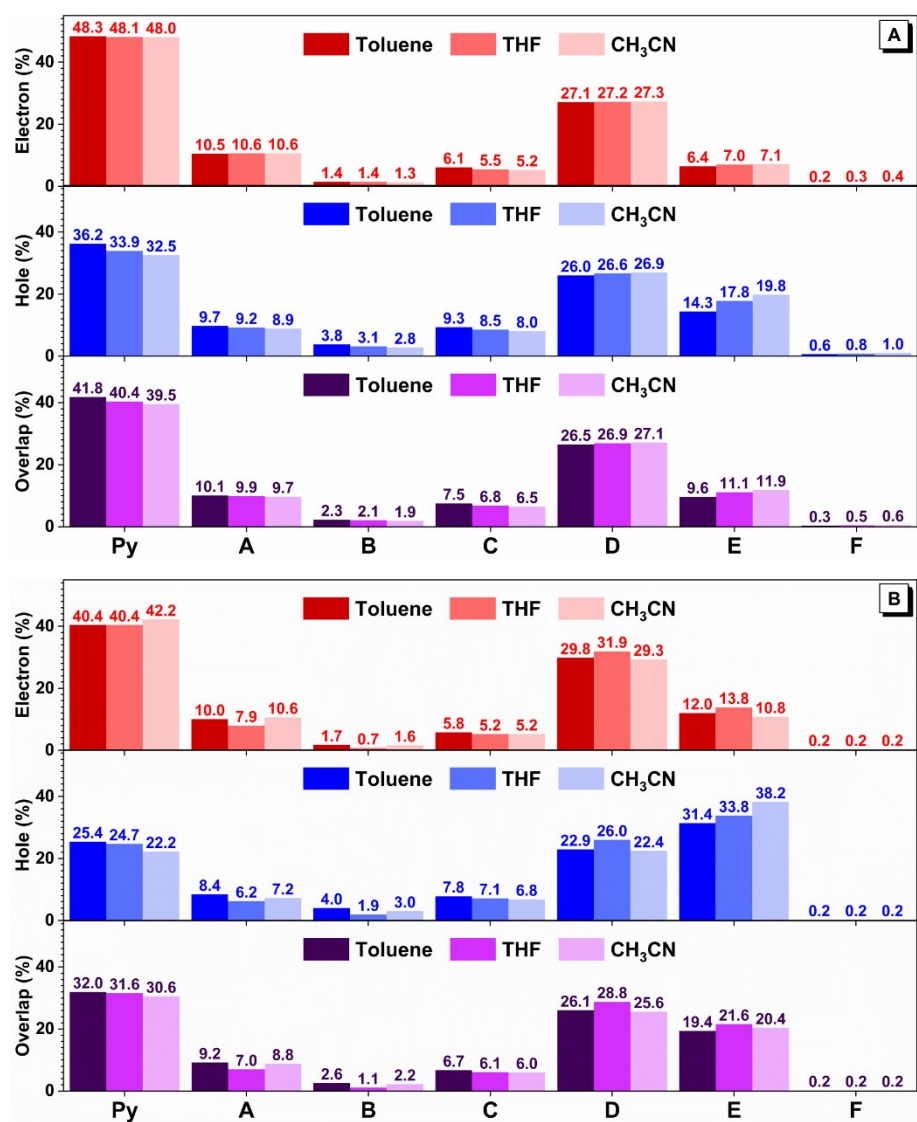


Figure S9. In three selected solvents, The distribution ratio of hole, electron and their overlap for (A) TPP-3C and (B) TPP-PI.

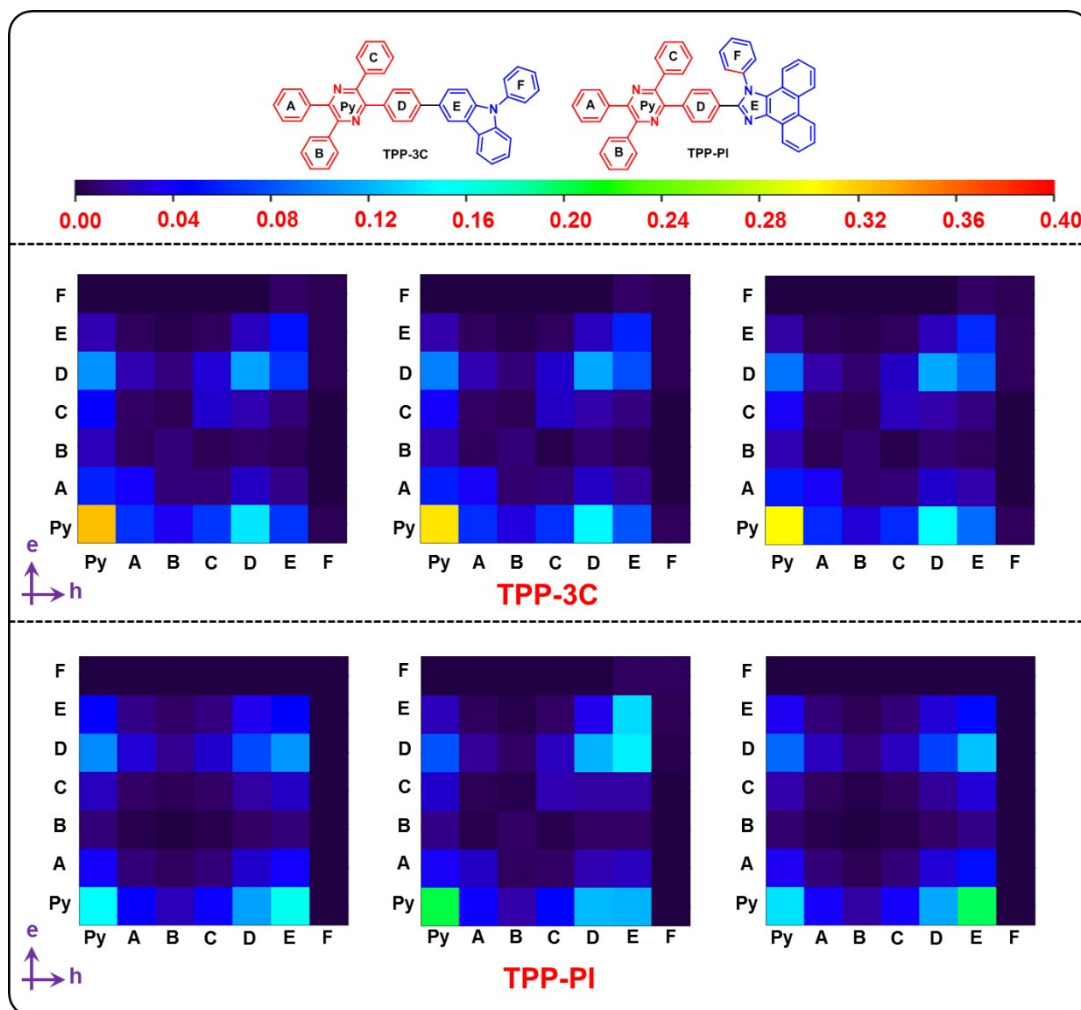


Figure S10. The 7-fragment TDM of S_1 states for TPP-3C and TPP-PI in toluene (left), THF (middle) and CH_3CN (right).

Due to the weak donor 3C, TPP-3C with slight ICT feature only show a little difference on 7-fragment TDM in three solvents. However, for the TPP-PI with large conjugated donor PI, the change of its 7-fragment TDMs can be distinguished (Figure S10). In toluene, the main transition process of S_1 state is related to the {Py, Py} and {E, Py} with relatively large transition density. In THF, although the transition density of {Py, Py} increases, the transition density in the upper right region ({E, E} and {E, D}) also increases whilst that of {E, Py} decreases, which indicates the transition of S_1 state with large conjugation and delocalization. As the polarity further increases, the charge transfer process of {E, Py} becomes prominent, and all the local transition densities of {X, X} (X = Py, A, B, C, D, E and F) decreases.

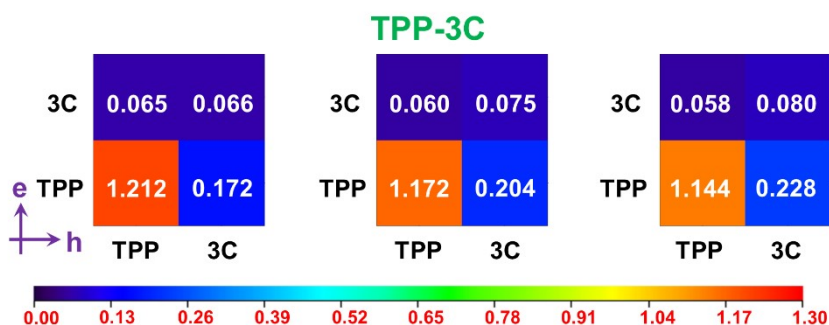


Figure S11. The 2-fragment TDM of S_1 states for TPP-3C in toluene (left), THF (middle) and CH_3CN (right).

To distinguish the S_1 transition change of TPP-3C, its 2-fragment TDM are described in Figure S11. Remarkably, the local transition of TPP is always dominated on the S_1 states. As the solvent polarity increases, the local transition density of {TPP, TPP} decreases slightly accompanying with a little increase of {3C, 3C} and {3C, TPP} density.

Briefly, the reduced contribution of TPP on the whole S_1 transition can prompt the luminescence of TPP-3C and TPP-PI even though their hole-electron distributions and TDM show the various change dependent on polarity.

Part 7. The proposed guideline for PEE

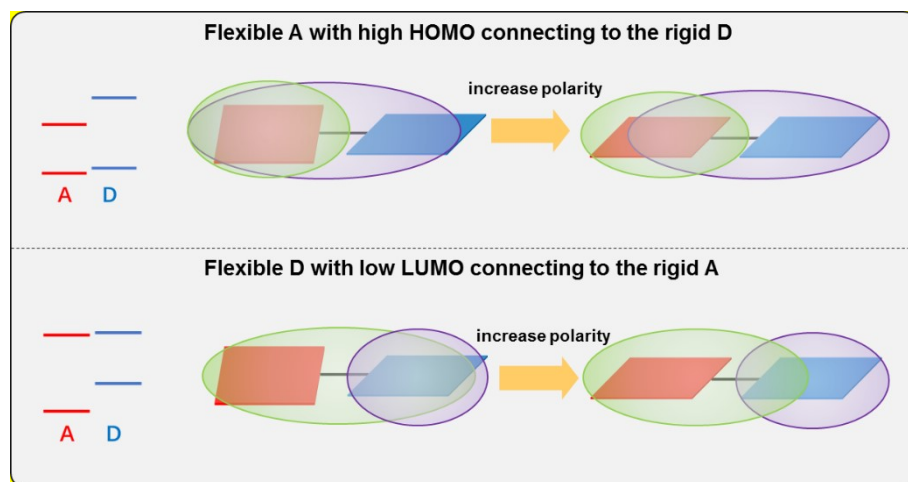


Figure S12. The schematic diagram of hole-electron distribution for our proposed PEE strategy.

Based on this investigation, we consider that the new A units that can achieve PEE should have the feature similar to TPP (flexible structure, weak electron-deficiency with high HOMO level). So the solvent polarity will change the hole-electron overlap on the flexible A units, which realizes the PEE. Along this way, if the new D unit with flexible structure and low LUMO level connects with a rigid A, the hole of the new molecule will locate mostly on the D while the electron will distribute on the whole molecules. In this situation, the significant hole-electron overlap on the flexible D unit brings the poor luminescence. Finally, the PEE can be also achieved because the hole-electron overlap on flexible D units will be impacted by the solvent polarity.